



# Fission fragment angular distribution measurements for $^{16}\text{O} + ^{194}\text{Pt}$ reaction at energies near the Coulomb barrier

E. Prasad <sup>a,b,\*</sup>, K.M. Varier <sup>b</sup>, R.G. Thomas <sup>c</sup>, A.M. Vinodkumar <sup>b</sup>,  
K. Mahata <sup>c</sup>, S. Appannababu <sup>d</sup>, P. Sugathan <sup>e</sup>, K.S. Golda <sup>e</sup>,  
B.R.S. Babu <sup>b,f</sup>, A. Saxena <sup>c</sup>, B.V. John <sup>c</sup>, S. Kailas <sup>c</sup>

<sup>a</sup> *Department of Physics, School of Mathematical and Physical Sciences, Central University of Kerala, Nileshtar, 671328, India*

<sup>b</sup> *Department of Physics, University of Calicut, Calicut, 673635, India*

<sup>c</sup> *Nuclear Physics Division, Bhabha Atomic Research Centre, Mumbai, 400085, India*

<sup>d</sup> *Department of Physics, Faculty of Science, The M. S. University of Baroda, Vadodara, 390002, India*

<sup>e</sup> *Inter University Accelerator Centre, Aruna Asaf Ali Marg, Post Box 10502, New Delhi, 110067, India*

<sup>f</sup> *Department of Physics, Sultan Qaboos University, Muscat, Oman*

Received 31 January 2012; received in revised form 7 March 2012; accepted 19 March 2012

Available online 28 March 2012

## Abstract

Fission fragment angular distributions have been measured for  $^{16}\text{O} + ^{194}\text{Pt}$  reaction forming the compound system  $^{210}\text{Rn}$ , in the laboratory energy range from 79 to 90 MeV. The measured fission fragment anisotropies as a function of  $E_{c.m.}/V_B$  are compared with the predictions of standard saddle point statistical model (SSPM). Anisotropies calculated using the average excitation energy and angular momentum values could not reasonably fit the experimental data. Statistical model calculations were performed using the PACE with modified fission barrier and level density parameters. Fission probability, evaporation residue cross section and neutron multiplicity were simultaneously used to fix the statistical parameters. Model calculations incorporating the chance nature of fission decay and scaled values of the rotating finite range model (RFRM) moment of inertia could reasonably fit the fragment angular anisotropies.

© 2012 Elsevier B.V. All rights reserved.

\* Corresponding author at: Department of Physics, School of Mathematical and Physical Sciences, Central University of Kerala, Nileshtar, 671328, India.

*E-mail address:* [prasad.e.nair@gmail.com](mailto:prasad.e.nair@gmail.com) (E. Prasad).

**Keywords:** NUCLEAR REACTIONS  $^{194}\text{Pt}(^{16}\text{O}, \text{F})$ ,  $E = 79\text{--}90$  MeV; measured fission  $E$  (fragment),  $I$  (fragment,  $\theta$ ); calculated  $\sigma(\theta)$ , fission barrier, ER  $\sigma$ , neutron multiplicity using PACE, anisotropy using SSPM (Statistical Saddle Point Model), RFRM (rotating finite range model) moments of inertia; deduced fission fragments  $\sigma(\theta)$ ,  $\sigma$ , fission probability, level density parameters

## 1. Introduction

Fission fragment angular distribution is an effective probe to understand the dynamics of heavy ion induced fusion–fission reactions. Experimentally it is well established that the fragments are emitted preferentially in the forward and backward directions with respect to the beam direction. The angular anisotropy ( $A$ ) is defined as the ratio of differential cross section of the fragments along the beam direction ( $W(180^\circ)$  or  $W(0^\circ)$ ) to that in the perpendicular ( $W(90^\circ)$ ) direction. Fragment angular distribution mainly depends on the angular momentum brought in by the projectile in heavy ion fusion reactions and the fraction of this angular momentum converted into orbital angular momentum between the fragments [1]. The experimental angular distribution and anisotropy data were generally explained using Statistical Saddle Point Model (SSPM) [2], in which, the fragment anisotropy is related to the moment of inertia, the total angular momentum of the compound nucleus (CN) and the temperature at the saddle point.

The observation of anomalously large angular anisotropies in heavy ion induced fission reactions involving actinide targets resulted in a renewed interest in this topic [3–6]. The admixture of non-compound nuclear (NCN) processes such as quasifission [7–9], fastfission [10,11] and pre-equilibrium fission [12] with the compound nuclear process was interpreted to be the possible reason for this anomalous behaviour. The entrance channel mass asymmetry ( $\alpha$ ) with respect to the Businaro–Gallone [13,14] critical mass asymmetry ( $\alpha_{BG}$ ) also plays a very important role in the reaction dynamics [12].

Considerable effort has been invested in recent years to understand the possible influence of shell closure on fusion–fission dynamics. In nuclei, shell closure provides extra stability against fission. The stabilizing effects of shell closure is the possible reason for the existence of super heavy elements. It was well established that the shell corrections [15] lead to double humped fission barrier in the actinide region. However, in  $\sim 200$  mass region, the shell corrections are not expected to produce any secondary minimum in the nuclear potential, as the liquid drop energy varies steeply with deformation. Even though significant shell corrections in fission barrier heights as a function of deformation are predicted in mass  $\sim 200$  region [16,17], experimental evidences are rather scarce. Vermeulen et al. [18] have carried out a comprehensive study of production cross sections of proton-rich evaporation residues near the  $N = 126$  neutron shell. These studies revealed a surprisingly low stabilizing influence of the spherical  $N = 126$  shell which is in agreement with the general observation that the shell effects wash out at higher excitation energies. However, anomalous fission fragment angular anisotropies were reported for  $^{12}\text{C} + ^{198}\text{Pt}$  system (forming the CN  $^{210}\text{Po}$  with neutron number  $N = 126$ ) and normal anisotropies for  $^{12}\text{C} + ^{198}\text{Pt}$  ( $^{206}\text{Po}$ ,  $N = 122$ ) by Shrivastava et al. [19]. The authors conjectured that the possible reduction of the moment of inertia at the saddle point, due to shell effects in the potential energy surface, could be the reason for the increase in fragment angular anisotropies for the former system. Djerroud et al. [20] also pointed out the possible importance of shell corrections at the saddle point from a systematic study of fusion around 190 mass region. Subsequent measurements in  $^{19}\text{F} + ^{194,198}\text{Pt}$  reactions [21] forming the compound systems  $^{213}\text{Fr}$  ( $N = 126$ ) and  $^{217}\text{Fr}$  ( $N = 130$ ) further revealed the role of shell corrections in fission dynamics at higher

energies. The multichance nature of fission decay was properly treated in the analysis of the data in their analysis. However, the experimental data on  $^{19}\text{F} + ^{197}\text{Au}$  [22] and  $^{18}\text{O} + ^{197}\text{Au}$  reactions [23] were successfully explained using the SSPM frame work. Hence it is very imperative to understand the role of shell corrections as well as the chance nature of fission in fusion–fission reactions, especially in mass  $\sim 200$  region. The proper understanding of the role of shell corrections in fission barrier heights at higher excitations would be extremely helpful in predicting the region of relatively stable superheavy elements.

Here, we report the fission fragment angular distribution measurements in  $^{16}\text{O} + ^{194}\text{Pt}$  ( $\alpha = 0.847$ ) reaction populating the CN  $^{210}\text{Rn}$  ( $\alpha_{BG} = 0.857$ ,  $N = 124$ ). The measurements were performed in the energy range 5% below to 10% above the Coulomb barrier.

## 2. Experiment

The experiment was performed using the general purpose scattering chamber of the BARC-TIFR 14UD Pelletron accelerator facility at Mumbai.  $^{16}\text{O}$  beam (dc) in the energy range 79–90 MeV was used to bombard  $^{194}\text{Pt}$  target of thickness  $300 \mu\text{g}/\text{cm}^2$  with  $20 \mu\text{g}/\text{cm}^2$  thick carbon backing. The fission fragments were collected using three  $\Delta E$ – $E$  silicon detector telescopes consisting of 15–20  $\mu\text{m}$  thick  $\Delta E$  detectors and 300–500  $\mu\text{m}$  thick  $E$  detectors with a 5.0 mm collimator. These telescopes were placed at a distance of 13.6 cm from the target, on the same movable arm of the 1 meter diameter scattering chamber. Two silicon surface barrier detectors were mounted at an angle of  $\pm 20^\circ$  with respect to the beam direction, at a distance of 42 cm from the target position. The counts from these detectors were used to monitor beam incidence. They were also used for the normalization of the fission yields and estimation of the absolute differential cross sections. The angular distribution of the fission fragments were measured at  $10^\circ$  intervals from  $80^\circ$  to  $170^\circ$  in the laboratory frame and the trigger of the data acquisition was derived from signals of the  $\Delta E$  detectors. The relative solid angles of the telescopes were taken into account by measuring the data at overlapping angles. Most of the fragments were stopped at the thin  $\Delta E$  detectors itself and fragments reaching the  $E$  detectors were well separated in energy from elastic, quasielastic and other channels.

## 3. Analysis and results

The measured fission fragment angular distributions were transformed from laboratory to centre-of-mass frame using Viola systematics for symmetric fission [24]. Energy loss corrections of the beam in the half target thickness were applied before the conversion to centre-of-mass. Rutherford scattering events in the monitor detectors were used for the normalization to obtain the absolute fission cross sections. The differential fission cross section was calculated using the expression

$$W(\theta_{cm}) \propto \frac{d\sigma_{fis}}{d\Omega} = \frac{1}{2} \frac{Y_{fis}}{Y_{mon}} \left( \frac{d\sigma}{d\Omega} \right)_R \frac{\Omega_{mon}}{\Omega_{fis}} G \quad (1)$$

where  $G$  is the Jacobian of laboratory frame to centre-of-mass frame transformation and  $Y_{fis}$  and  $Y_{mon}$  are the yields recorded by the fission detector and monitor (Rutherford) detector, respectively.  $\Omega_{fis}$  and  $\Omega_{mon}$  are the solid angles subtended by the fission detector and monitor detector, respectively.  $(\frac{d\sigma}{d\Omega})_R$  is the differential Rutherford cross section in the laboratory system.

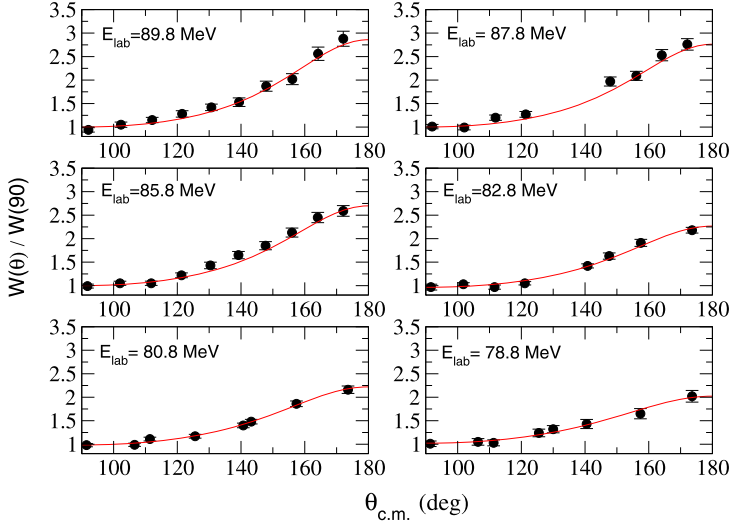


Fig. 1. Fission fragment angular distributions at different beam energies for  $^{16}\text{O} + ^{194}\text{Pt}$  reaction. The continuous red line is the fit using standard expression for angular distribution [25]. (For interpretation of the references to color in this figure legend, the reader is referred to the web version of this article.)

Total fission cross section was obtained by integrating the differential cross section  $\frac{d\sigma_{fis}}{d\Omega}$ . The angular distributions were fitted using the standard expressions [1,25]. Under the standard [1,25] assumptions, angular distributions can be represented as

$$W(\theta) = \sum_{J=0}^{\infty} (2J+1)T_J \frac{\sum_{K=-J}^J \frac{1}{2}(2J+1)d_{0K}^J(\theta)^2 \exp\left[\frac{-K^2}{2K_0^2(J)}\right]}{\sum_{K=-J}^J \exp\left[\frac{-K^2}{2K_0^2(J)}\right]} \quad (2)$$

where,  $T_J$  is the transmission coefficient for fusion of the  $J$ th partial wave,  $K_0^2 = \frac{I_{eff}}{\hbar^2} T$ , is the variance of the  $K$  distribution and  $I_{eff}$  is the effective moment of inertia at the saddle point. The saddle point temperature is calculated using the expression  $T = \sqrt{E^*/a}$ , where  $E^*$  is the excitation energy of the fissioning system ( $E^* = E_{c.m.} + Q - B_f(l) - E_{rot}(l) - E_n$ ) and ‘ $a$ ’ is the level density parameter. Here,  $E_{c.m.} + Q$  is the excitation energy of the CN,  $B_f(l)$  and  $E_{rot}(l)$  are the ‘ $l$ ’ dependent fission barrier height and rotational energy, respectively. The  $E_n$  is the reduction in the excitation energy of the system by evaporating neutrons. The  $I_{eff}$ ,  $B_f$  and  $E_{rot}$  were calculated by using rotating finite range model [26]. The angular distributions of the fragments at different beam energies along with the fits are shown in Fig. 1. Fission fragment angular anisotropies ( $A = \frac{W(180^\circ)}{W(90^\circ)}$ ) were hence obtained from the above fit. Table 2 gives the experimental fragment anisotropies and fission cross sections at different beam (centre-of-mass) energies.

In SSPM the fragment angular anisotropy is related to the angular momentum of the fissioning system  $J$  at the saddle point and the projection of this total angular momentum on the nuclear symmetry axis  $K$ . In the simplified form the fragment angular anisotropy is given by the approximate expression

$$A = 1 + \frac{\langle l^2 \rangle}{4K_0^2} \quad (3)$$

Table 1  
Experimental fission fragment angular anisotropy and fission cross section for  $^{16}\text{O} + ^{194}\text{Pt}$  reaction at different centre-of-mass energies.

$E_{c.m.}$ (MeV)	$A_{expt}$	$\sigma_{fiss}$ (mb)
72.8	$1.981 \pm 0.14$	$17.0 \pm 1.8$
74.6	$2.256 \pm 0.12$	$47.1 \pm 2.7$
76.5	$2.351 \pm 0.09$	$75.7 \pm 4.4$
79.3	$2.697 \pm 0.11$	$161.4 \pm 11.2$
81.1	$2.763 \pm 0.12$	$256.0 \pm 21.5$
83.0	$2.858 \pm 0.15$	$316.3 \pm 26.5$

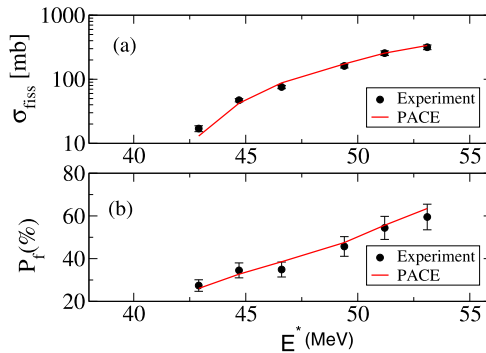


Fig. 2. Fission probability and fission cross sections for  $^{16}\text{O} + ^{194}\text{Pt}$  reaction plotted against CN excitation energy. The solid line is the statistical model fit to the experimental data.

The mean square angular momentum ( $\langle l^2 \rangle$ ) values of the fissioning nuclei were calculated using statistical model code PACE [27] in trace back mode using fusion spin distributions as the input. The fusion spin distributions were obtained using the coupled channel code CCFULL [28] by fitting the experimental fusion cross section (sum of evaporation residue (ER) cross section and fission cross section). ER cross section for this reaction was measured in a separate experiment [29]. The broadening of the angular momentum at near barrier energies [30] were taken into account in CCFULL calculations by including the rotational couplings of the target nuclei. The calculations assuming average values of excitation energy and angular momentum [3,31], however, failed to explain the experimental results satisfactorily. This may be due to the multichance nature of the fission decay, a dominant decay mode in pre-actinide region. If multi-chance fission is a dominant decay mode, fission can take place from the CN itself or after one or few neutron emission. Hence, the angular momentum distributions and temperature of the fissioning nuclei will be very different. Experimentally measured angular distribution, hence, contains contributions from various stages of these decay and calculations assuming average values of angular momentum and excitation energy may yield erroneous results.

As the experimental data considered in the present work is in the excited energy range 42–53 MeV, statistical model analysis is valid. We also verified in our earlier measurements [29,32] that the contribution from NCN events are absent in  $^{16}\text{O} + ^{194}\text{Pt}$  reaction. In order to reduce the ambiguities in choosing the statistical parameters (fission barrier height ( $B_f(l)$ ), the ratio of level density parameter at saddle point and equilibrium deformation ( $\frac{a_f}{a_n}$ ), and level density parameter at equilibrium deformation ( $a_n$ )) to fit the experimental data, ER cross section, fission

Table 2  
Different parameters of the reaction  $^{16}\text{O} + ^{194}\text{Pt}$ .

$E_{c.m.}$ (MeV)	$E_{CN}^*$ (MeV)	$\langle l^2 \rangle$	$B_f/T$	PEF (%)
72.8	42.9	156.2	8.585	0.12
74.6	44.7	226.6	9.285	0.19
76.5	46.6	298.9	9.919	0.32
79.3	49.4	425.5	11.491	0.70
81.1	51.2	516.1	12.629	0.96
83.0	53.1	560.1	13.366	1.37

cross section and pre-scission neutron multiplicities were simultaneously fitted using PACE in the present calculations. To the best of our knowledge,  $\nu_{pre}$  values of  $^{16}\text{O} + ^{194}\text{Pt}$  system are not reported in literature. Hence,  $\nu_{pre}$  values were calculated using the systematics of Saxena et al. [33]. The form of the fission barrier used in the calculation is given by

$$B_f(l) = B_f^{LDM}(l) - \Delta n + k_f \Delta n \quad (4)$$

where  $B_f^{LDM}(l)$  is the liquid drop component of the fission barrier taken from Ref. [26],  $\Delta n$  is the shell correction at the ground state deformation and  $k\Delta n$  is the shell correction at saddle point deformation, with  $k$  as the scaling factor. An energy dependent form [34] of shell correction  $a_x = \tilde{a}[1 + \frac{\Delta x}{U}(1 - e^{-\eta U_x})]$  with the asymptotic value  $\tilde{a} = A_{CN}/9$  was used for the level density, in the present calculations ( $x = n$  for ground state and  $x = f$  for saddle point deformations). Here  $\eta$  is the damping factor (in the present case we used  $\eta = 0.054 \text{ MeV}^{-1}$  taken from literature [34, 35]), which is a measure of the rate at which shell effects melt away with increase in excitation energy and  $U$  is the thermal energy.

Statistical model calculations were performed by varying the values of  $k_f$  and  $\frac{a_f}{a_n}$  to simultaneously fit the ER cross section, fission cross section and pre-fission neutron multiplicities. Experimental fission probability and fission cross sections are plotted against CN excitation energy is shown in Fig. 2(a) and (b). The solid line is the statistical model fit to the experimental data. The best fit to the experimental values were obtained for  $k_f = 0.762$  and  $\frac{a_f}{a_n} = 0.983$ . After fixing the statistical model parameters, SSPM calculations have been performed for the fission fragments angular anisotropies. As mentioned earlier, in pre-actinide region as the fission barrier heights are comparable with neutron separation energies, multichance fission decay contributes substantially to the decay mode. Hence, the excitation energy and angular momentum distributions of the fissioning nuclei for each chance fission were taken from PACE [27] predictions.  $I_{eff}$ -values were taken from Ref. [26]. In Table 2 we have shown different parameters of the system  $^{16}\text{O} + ^{194}\text{Pt}$ .

The experimental anisotropies were compared with SSPM calculations as a function of centre-of-mass energy in Fig. 3. It may be noted that saddle point model calculations using the chance distributions taken from PACE fail to explain the experimental data at all energy points. Hence the Sierk's  $I_{eff}$  value has been normalized by multiplying a suitable factor to fit the experimental data in the energy range studied. The final  $I_{eff}$  values were obtained by averaging over the entire energy range. A multiplicative factor of  $1.10 \pm 0.37$  was required to fit the anisotropy data for  $^{16}\text{O} + ^{194}\text{Pt}$  reaction in the energy range studied in the present work, with the errors representing the standard deviations. It may also be noted that the calculation deviates from the experimental data at the highest energy, which may be due to the dissipative effects [29] and subsequent enhancement in pre-scission neutron emission, which we have not considered explicitly in the present model calculations.

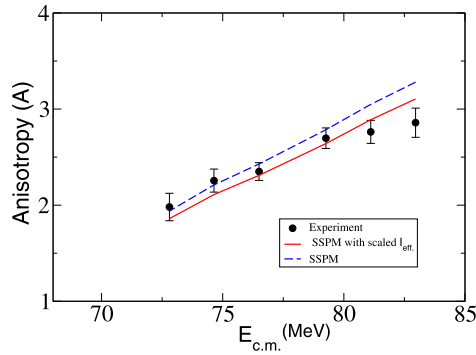


Fig. 3. Fission fragment angular anisotropies for  $^{16}\text{O} + ^{194}\text{Pt}$  reaction plotted against centre-of-mass energies. SSPM calculations using the chance distribution from the PACE3 output is shown as blue dotted line. The calculations using scaled  $I_{eff}$  reasonably explain the data at all energies (red solid line). (For interpretation of the references to color in this figure legend, the reader is referred to the web version of this article.)

#### 4. Discussion

We have analysed the measured fission fragment angular distribution data using the framework of SSPM for  $^{16}\text{O} + ^{194}\text{Pt}$  reaction at energies around the Coulomb barrier. It may be noted that the contribution from pre-equilibrium fission (PEF) is negligible in the present system, in the energy range studied. At the highest energy, the probability of PEF (PEF probability is given by  $P_{PEF} = e^{-0.5B_f/T}$ ) is found to be 1.37%. It was also verified earlier [32] that the contribution from quasifission and fastfission are absent in the present reaction. SSPM calculations assuming the average values of CN excitation energies and angular momentum values failed to reproduce the experimental data reasonably well in the entire energy range studied in the present work. Statistical model calculations were performed using PACE with modified fission barrier and level density parameters. Significant shell corrections required to fit the experimental data in the present system hints the role of shell corrections at ground state and saddle point deformations in mass  $\sim 200$  region. Similar results were reported earlier in  $^{12}\text{C} + ^{194,198}\text{Pt}$  and  $^{19}\text{F} + ^{194,198}\text{Pt}$  systems [19,21] in this mass region. In mass  $\sim 200$  region, as the fission barrier height and neutron separation energies are comparable, multichance fission can play a significant role in the decay mode. Though there is substantial reduction in excitation energy during the neutron emission, the change in angular momentum brought in by the neutron emission is relatively very low. Since the fragment angular distribution depends upon the angular momentum distribution of the fissioning system, the calculations ignoring chance fission contributions yield erroneous results. In this work chance fission is properly treated to describe the fragment angular distribution data systematically. As our experimental data are limited from 42.9 to 53.1 MeV excitation energy only, we have not considered the enhanced pre-scission neutron multiplicity arising due to the dynamical delay, in this work. This is justified as the dynamical effects are not very significant at lower excitation energies [36].

#### 5. Summary

We measured the fission fragment angular distributions for the reaction  $^{16}\text{O} + ^{194}\text{Pt}$  and the results are compared with SSPM predictions. The multi-chance nature of fission decay has been included in the model calculations in this work. The chance distributions of the fission decay

were obtained using the statistical model code PACE, using fusion CN spin distribution as the input. The fission cross section, ER cross section and pre-scission neutron multiplicities were simultaneously fitted to constrain the statistical model parameters. Shell corrected fission barrier heights were used in the calculations. Though the contributions from non-compound nuclear events are absent in the present system, calculations assuming Sierk's  $I_{eff}$  value could not reproduce the experimental data satisfactorily at all energies.  $I_{eff}$  value increased by about 10% could reasonably represent the experimental data in the energy range studied. The present study thus hints the importance of multi-chance fission and shell corrected fission barrier heights in the analysis of fission fragment anisotropy data in mass  $\sim 200$  region. However, this work calls for more experimental efforts at near barrier energies to have a clear idea of the fission decay in pre-actinide nuclei.

## Acknowledgements

We acknowledge the cooperation and support received from Mr. A. Inker, Mr. R.V. Jangle and Dr. Ramachandran during the experiment. We thank the Pelletron crew of TIFR-BARC accelerator group for providing beams of excellent quality throughout the experiment. We thank N. Madhavan, S. Nath, Dr. B.P. Ajithkumar, Dr. A. Roy and Dr. B.R. Behera for their keen interest in this work. One of the authors (EP) gratefully acknowledges the award of research fellowship by University Grants Commission (UGC), New Delhi, for carrying out this work.

## References

- [1] R. Vandenbosch, J.R. Huizenga, Nuclear Fission, Academic Press, New York, 1973.
- [2] I. Halpern, V.M. Strutinsky, in: J.H. Martenes, et al. (Eds.), Proceedings of the Second United Nations International Conference on Peaceful Uses of Atomic Energy, vol. 15, Geneva, 1958, United Nations, Switzerland, 1958, p. 408.
- [3] S. Kailas, Phys. Rep. 284 (1997) 381, and references therein.
- [4] J.P. Lestone, A.A. Sonzogni, M.P. Kelly, R. Vandenbosch, Phys. Rev. C 56 (1997) 2907(R).
- [5] J.C. Mein, D.J. Hinde, M. Dasgupta, J.R. Leigh, J.O. Newton, H. Timmers, Phys. Rev. C 55 (1997) 995(R).
- [6] B.R. Behera, et al., Phys. Rev. C 64 (2001) 041602(R);  
B.R. Behera, et al., Phys. Rev. C 69 (2004) 064603.
- [7] W.J. Swiatecki, Phys. Scr. 24 (1981) 113.
- [8] S. Bjornholm, W.J. Swiatecki, Nucl. Phys. A 391 (1982) 471.
- [9] J.P. Blocki, et al., Nucl. Phys. A 459 (1986) 145.
- [10] C. Ngo, Prog. Part. Nucl. Phys. 16 (1986) 139.
- [11] C. Lebrun, F. Hanappe, J.F. LeColley, F. Lefebvres, C. Ngo, J. Peter, B. Tamain, Nucl. Phys. A 321 (1979) 207.
- [12] V.S. Ramamurthy, S.S. Kapoor, Phys. Rev. Lett. 54 (1985) 178.
- [13] U.L. Businaro, S. Gallone, Nuovo Cimento 5 (1957) 315.
- [14] M. Abe, KEK Report No. 86-26, KEK TH-28, 1986.
- [15] V.M. Strutinsky, Nucl. Phys. A 95 (1967) 420.
- [16] U. Mosel, H.W. Schmitt, Phys. Rev. C 4 (1971) 2185.
- [17] M. Bolsterli, O.E. Fiset, J.R. Nix, J.L. Newton, Phys. Rev. C 5 (1972) 1050.
- [18] D. Vermeulen, H.G. Clerc, C.C. Sahn, K.H. Schmidt, J.G. Keller, G. Munzenberg, W. Reisdorf, Z. Phys. A 318 (1984) 157.
- [19] A. Shrivastava, S. Kailas, A. Chatterjee, A.M. Samant, A. Navin, P. Singh, B.S. Tomar, Phys. Rev. Lett. 82 (1999) 699.
- [20] B. Djerroud, et al., Phys. Rev. C 61 (2000) 024607.
- [21] K. Mahata, S. Kailas, A. Shrivastava, A. Chatterjee, P. Singh, S. Santra, B.S. Tomar, Phys. Rev. 65 (2002) 034613.
- [22] R. Tripathi, K. Sudarshan, S. Sodaye, A.V.R. Reddy, K. Mahata, A. Goswami, Phys. Rev. C 71 (2005) 044616.
- [23] S. Appannababu, S. Mukherjee, N.L. Singh, P.K. Rath, G. Kiran Kumar, R.G. Thomas, S. Santra, B.K. Nayak, A. Saxena, R.K. Choudhury, K.S. Golda, A. Jhingan, R. Kumar, P. Sugathan, Hardev Singh, Phys. Rev. C 80 (2009) 024603.

- [24] V.E. Viola, K. Kwiatkowski, M. Walker, *Phys. Rev. C* 31 (1985) 1550.
- [25] B.B. Back, R.R. Betts, J.E. Gindler, B.D. Wilkins, S. Saini, M.B. Tsang, C.K. Gelbke, W.G. Lynch, M.A. McMahan, P.A. Baisden, *Phys. Rev. C* 32 (1985) 195.
- [26] A.J. Sierk, *Phys. Rev. C* 33 (1986) 2039.
- [27] A. Gavron, *Phys. Rev. C* 21 (1980) 230.
- [28] K. Hagino, N. Rowley, A.T. Kruppa, *Comput. Phys. Commun.* 123 (1999) 143.
- [29] E. Prasad, et al., *Phys. Rev. C* 84 (2011) 064604.
- [30] R. Vandenbosch, *Annu. Rev. Nucl. Part. Sci.* 42 (1983) 447.
- [31] L.C. Vaz, J.M. Alexander, *Phys. Rep.* 97 (1983) 1.
- [32] E. Prasad, et al., *Phys. Rev. C* 81 (2010) 054608.
- [33] A. Saxena, A. Chatterjee, R.K. Choudhury, S.S. Kapoor, D.M. Nadkarni, *Phys. Rev. C* 49 (1994) 932.
- [34] A.V. Ignatyuk, M.G. Itkis, V.N. Okolovich, G.N. Smirenki, A. Tishin, *Sov. J. Nucl. Phys.* 21 (1975) 255.
- [35] K. Mahata, S. Kailas, A. Shrivastava, A. Chatterjee, A. Navin, P. Singh, S. Santra, B.S. Tomar, *Nucl. Phys. A* 7200 (2003) 209.
- [36] B.B. Back, D.J. Blumenthal, C.N. Davids, D.J. Henderson, R. Hermann, D.J. Hofman, C.L. Jiang, H.T. Penttila, A.H. Wuosmaa, *Phys. Rev. C* 60 (1999) 044602.